Supporting information for: Impact of iron coordination isomerism on pyoverdine recognition by the FpvA membrane transporter of *Pseudomonas aeruginosa*

Benjamin Bouvier* and Christine Cézard

Laboratoire de Glycochimie, des Antimicrobiens et des Agroressources, CNRS UMR7378/Université de Picardie Jules Verne, 10, rue Baudelocque, 80039 Amiens Cedex, France.

E-mail: benjamin.bouvier@u-picardie.fr

Stereochemistry of iron chelation

Octant sign and plane methods. In the octant sign (OS) method, one of the chelate ring is placed so that its two donor atoms lie in the xy plane, at coordinates $(-x, +y)$ and $(+x, +y)$. Since the donor atoms define a tetrahedron, there exist three distinct combinations of four donor atoms that are coplanar; the plane that contains the two previously mentioned donor atoms also contains two other atoms (which do not necessarily belong to the same ring). These are placed at coordinates $(-x, -y)$ and $(+x, -y)$ and define the y axis. The z axis is obtained from the cross product of x and y. The origin of the coordinate system is positioned at the Fe^{3+}ion and eight octants are defined, each of which is tagged by the

*To whom correspondence should be addressed

sign of xyz, where x, y and z are the coordinates of any point in that octant (see figure S1). The chirality can then be inferred from the sign of the octant to which the second ring belongs: positive for Λ and negative for Δ. Another method to determine the chirality of an octahedral complex is to identify the aforementioned three planes containing four of the donor atoms each; these planes are aABc, abBc and AbcC for Λ enantiomers, and aBCc, AaCb, ABbc for Δ enantiomers.

Equivalence of Φ, OS and plane methods. As a validation of the conformational coordinate Φ upon which bias is applied to trigger the reversible transition from Λ to Δ in our simulations, we have compared its ability to characterize the chirality of structures encountered along the pathways with those of the OS and plane methods. We found all methods to be equivalent when applied to hexadentate coordinations, and able to distinguish the latter from compounds of lower coordination (figure S2). Moremover, the Φ angle is expected to behave more reliably in conformations that deviate significantly from canonical hexadentate arrangements.

Ability of Φ to describe possible isomers within each chirality. 16 isomers of a given octahedral coordination complex (8 Λ and 8 Δ), obtained by interchanging the positions of the chelating atoms, are theoretically possible.[S1] Although not all of these conformations are sterically feasible, simulated annealing calculations by Wasielewski et al on PVDI/Ga^{3+} complexes have shown several to be.[S2] However, comparing possible isomer structures and data harvested from NMR experiments, these authors have shown that Λ-PVDI exists predominantly in one state (dubbed Λ-4), which is also the conformation in which PVDI is found when bound to FpvA. In the case of Δ-PVDI, the authors suspect a single conformer to be present in solution, but structural uncertainties prevent them from discriminating between two equally probable conformations (Δ-7 and Δ-8), with a third, marginally less probable one (Δ-5) coming very close behind. Since these three conformations differ only by the rotation of the Cδ-Nϵ bond of each of the two FoOHOrn moieties which has very little effect on the peptide backbone, the authors select Δ-8 as the sole rep-

resentative of Ga^{3+}-binding Δ-PVDI. Using the notations of Wasielewski et al, the dihedral angles used in this work to define the conformational coordinate Φ describe the transition from Λ-4 to Δ-5 conformations. Considering the experimental results on PVDI-Ga^{3+} complexes described in the previous paragraph, this is quite realistic even considering possible conformational discrepancies between Ga^{3+} and Fe^{3+}-binding siderophores. In addition, the non-biased simulations of Λ and Δ PVDI and PVD_{G173} (either free or bound to FpvA) that we have performed over sizeable timescales show all three dihedral angles involved in Φ to be equivalent (which would not hold true if transitions between isomers of a given chirality occurred) – see figure S3. As such, even if our conformational coordinate Φ is not general enough to account for all possible conformers, it describes the experimentally observed ones and should not meaningfully bias the pathway, making its ease of computing a very worthwhile tradeoff.

Additional computational details

Spin state of Fe^{3+} bound to pyoverdines. The $[FeL_6]^{3+}$ ground state complex, consisting of six ligands L bound to Fe^{3+}, can adopt three spin states: the low-spin doublet ($S = 1/2$), the intermediate-spin quartet ($S = 3/2$) and the high-spin sextet ($S = 5/2$). While the five $3d$ orbitals are degenerate in the isolated, gas-phase Fe^{3+} ion, in the presence of an electric field created by surrounding ligands, the degeneracy of the $3d$ orbitals is raised and a splitting of the latter is observed. For symmetry reasons, the d_{xy}, d_{xz} and d_{yz} orbitals will be less destabilized than the d_{z^2} and $d_{x^2-y^2}$ ones. Available crystal structures of pyoverdines reveal that complexation around Fe^{3+} exhibits an octahedral geometry.[S3] For the O_h point group, d_{xy}, d_{xz} and d_{yz} belong to the e_g irreductible representation, while d_{z^2} and $d_{x^2-y^2}$ belong to t_{2g}. The energy gap between the two sets of $3d$ orbitals is denoted Δ_{oct}. The magnitude of this energy gap is determined by the strength of the field created by the surrounding ligands. Pyoverdines possess three asymmetrical bidendate Fe^{3+} binding sites, i.e. the chromophore and two hydroxy-formyl-ornithines. The coordination sites of Fe^{3+} are thus occupied by six

oxygen atoms belonging to one catecholate and two hydroxamate functions, four of which bear a negative charge. Both catecholate[S4,S5] and hydroxamate[S6] functions are weak-field ligands, hence Δ_{oct} is low for such $Fe^{3+}[O\cdots X]_6$ complexes and the corresponding electronic configuration of iron is $t_{2g}^3 e_g^2$. Consequently, in all our *ab initio* calculations, the considered $[Fe^{3+}L_6]$ complexes are high spin, i.e. open shell systems featuring a ferric ion with five unpaired electrons ($S = 5/2$) and a multiplicity of six. In addition, there is no spin crossover (interchange between high spin and low spin states) in the systems considered in this study.[S7]

***Ab initio* DFT calculations.** All *ab initio* calculations were performed using Gaussian 09[S8] in the gas phase. Full geometry optimizations were performed with both the B3LYP and M06 functionals, using the 6-31G* basis set. Frequency calculations were systematically performed to verify the true nature of minimum points. The Gibbs free energy estimate was performed at a pressure of 1 atm and a temperature of 298 K.

Molecular dynamics forcefields and parameters. All-atom simulations were performed under conditions of constant temperature (300 K) and pressure (1 bar) using the Nosé-Hoover ($\tau = 0.5$ ps, applied separately to FpvA, membrane and solvent) and semi-isotropic Parrinello-Rahman algorithms ($\tau = 2$ ps, $\beta = 4.5 \times 10^{-5}$ bar^{-1}, independent treatment of xy and z components). Coulomb interactions were computed using the particle-mesh Ewald method with a 1.2 nm real-space cutoff. The same cutoff value was employed for Van der Waals interactions. The equations of motion were integrated every 2 fs. Bonds involving hydrogen atoms were constrained using LINCS.

Coarse-grained simulations used a reaction-field framework (cutoff 1.1 nm, $\epsilon_r = 15$, $\epsilon_{field} = \infty$) for electrostatics and potential-shift Verlet (cutoff 1.1 nm) for Van der Waals interactions. Temperature was maintained at 300 K and pressure at 1 bar using velocity rescaling ($\tau = 1.0$ ps, applied separately to solute and solvent) and semi-isotropic Parrinello-Rahman algorithms ($\tau = 12$ ps, $\beta = 3 \times 10^{-4}$ bar^{-1}, independent treatment of xy and z components). The equations of motion were discretized in 20 fs timesteps unless otherwise specified.

All simulations were performed using GROMACS 5.[S9] The all-atom topology for the system mixes forcefields derived from AMBER and GLYCAM[S10] which use different conventions for the scaling of nonbonded 1-4 interactions. Since GROMACS cannot accomodate more than one convention simultaneously, the AMBER convention was retained; while this could result in sugar rotamer populations that deviate from experiments, it is not expected to majorly impact the dynamics of the overall system.[S10] Metadynamics simulations were performed and analyzed using PLUMED 2.2.[S11]

Molecular dynamics simulations. The inner DPPE leaflet was removed from the all-atom starting structure of the *Pseudomonas aeruginosa* outer membrane, and the outer LPS leaflet conformation was coarse-grained. An inner leaflet of coarse-grained POPE was constructed using Insane[S12] and positioned with respect to the outer leaflet. The membrane patch was energy-minimized for 1000 steps of steepest descent; coarse-grained water was added on either side of the membrane, and 1000 further minimization steps were performed. MD simulations were then performed, in which the timestep was ramped up from 2 fs to 20 fs over 10 million timesteps; the system was further equilibrated for 50 ns using 20 fs timesteps. At this point, the system dimensions were $11.5 \times 8.3 \times 9.0$ nm and consisted of 72 LPS molecules, 180 POPE residues, 288 Ca^{2+} ions and 2353 water beads.

Residues 44 to 136, which belong to the TonB box, were removed from the experimental structure of the FpvA transporter (PDB id 2W75), upon which the structure was coarse-grained using Martinize. It was then inserted into the previously equilibrated membrane patch. The optimal insertion position on the membrane plane (x and y axes) was chosen as the one for which the smallest number of LPS moieties had to be removed, and in the orthogonal direction (z axis) so that the hydrophobic tails of lipopolysaccharide match the topmost ring (in the z direction) of hydrophobic residues on the FpvA barrel. Rather than being removed, the orientation and position of LPS molecules for which only a minority of grains intersected with FpvA beads were manually tweaked to avoid clashes. The system was then minimized to convergence, solvated with water, neutralized with chloride ions and

minimized for a further 2000 steps. It was simulated for 5 ns in 2 fs timesteps with fixed FpvA beads. These restraints were then removed, the timestep was ramped to 20 fs over 10 million timesteps and equilibrated for 50 ns in 20 fs timesteps. The simulation box at this point contained FpvA, 51 LPS molecules, 134 POPE molecules, 225 Ca^{2+}, 24 Cl^{-} ions and 4609 water beads and measured $11.4 \times 8.2 \times 11.7$ nm (the larger dimension along the z axis compared to the membrane patch box was required to accomodate the lid loops of the FpvA transporter).

The representative structure of the equilibrated coarse-grained system was backmapped to the all-atom AMBER/GLYCAM forcefields using Backward.[S13] The system was minimized to convergence, water and chloride ions were added and another round of minimization was performed. The system was equilibrated for 5 ns with fixed solutes, 5 ns with fixed protein, and 10 ns without constraints. At this point, the unit cell measured $11.1 \times 8.0 \times 9.3$ nm and contained 85860 atoms.

The all-atom starting structures for PVDI and PVD_{G173} bound to FpvA were resolvated and equilibrated as for *apo*-FpvA; the equilibrated box for FpvA/PVDI (resp. FpvA/PVD_{G173}) measured $11.0 \times 7.9 \times 9.6$ nm and contained 86037 particles (resp. $11.1 \times 8.0 \times 9.6$ nm and 86098 particles).

The PVDI (resp. PVD_{G173}) system consisted of the pyoverdine, 2505 (resp. 1692) water molecules and one Cl^{-} (resp. one K^{+}) ion in a truncated octahedral box of volume 77 nm^3 (resp. 53 nm^3).

The well-tempered metadynamics simulations used to accelerate the transitions of the isolated and FpvA-bound pyoverdines between the Λ and Δ isomers used the following parameters: frequency of hill addition 500 steps, hill width 2.5°, temperature 300 K, temperature bias factor 50.

Miscellaneous. All statistical analyses were performed using Scientific Python.[S14] Molecular graphics were produced using VMD[S15] and Pymol.[S16] All other plots and figures were generated using Matplotlib.[S17]

References

(S1) Teintze, M.; Hossain, M. B.; Barnes, C. L.; Leong, J.; Van der Helm, D. Structure of ferric pseudobactin: a siderophore from a plant growth promoting Pseudomonas. *Biochemistry* **1981**, *20*, 6446–6457.

(S2) Wasielewski, E.; Tzou, D.-L. L.; Dillmann, B.; Czaplicki, J.; Abdallah, M. A.; Atkinson, R. A.; Kieffer, B. Multiple conformations of the metal-bound pyoverdine PvdI, a siderophore of Pseudomonas aeruginosa: a nuclear magnetic resonance study. *Biochemistry* **2008**, *47*, 3397–3406.

(S3) Greenwald, J.; Nader, M.; Celia, H.; Gruffaz, C.; Geoffroy, V.; Meyer, J.-M. M.; Schalk, I. J.; Pattus, F. FpvA bound to non-cognate pyoverdines: molecular basis of siderophore recognition by an iron transporter. *Mol. Microbiol.* **2009**, *72*, 1246–1259.

(S4) Taylor, S. W.; Chase, D. B.; Emptage, M. H.; Nelson, M. J.; Waite, J. H. Ferric ion complexes of a DOPA-containing adhesive protein from Mytilus edulis. *Inorg. Chem.* **1996**, *35*, 7572–7577.

(S5) Yapo-Kicho, D.; Lagant, P.; Vergoten, G. The SPASIBA Force Field for Studying Iron-Tannins Interactions: Application to Fe3+/Fe2+ Catechol Complexe. *Int. J. Mol. Sci.* **2007**, *8*, 259–272.

(S6) Monzyk, B.; Crumbliss, A. L. Mechanism of ligand substitution on high-spin iron (III) by hydroxamic acid chelators. Thermodynamic and kinetic studies on the formation and dissociation of a series of monohydroxamatoiron (III) complexes. *J. Am. Chem. Soc.* **1979**, *101*, 6203–6213.

(S7) van Koningsbruggen, P. J.; Maeda, Y.; Oshio, H. *Spin crossover in transition metal compounds I*; Springer, 2004; pp 259–324.

(S8) Frisch, M. J.; Trucks, G. W.; Schlegel, H. B.; Scuseria, G. E.; Robb, M. A.; Cheeseman, J. R.; Scalmani, G.; Barone, V.; Mennucci, B.; Petersson, G. A.; Nakatsuji, H.; Caricato, M.; Li, X.; Hratchian, H. P.; Izmaylov, A. F.; Bloino, J.; Zheng, G.; Sonnenberg, J. L.; Hada, M.; Ehara, M.; Toyota, K.; Fukuda, R.; Hasegawa, J.; Ishida, M.; Nakajima, T.; Honda, Y.; Kitao, O.; Nakai, H.; Vreven, T.; Montgomery Jr., J. A.; Peralta, J. E.; Ogliaro, F.; Bearpark, M. J.; Heyd, J.; Brothers, E. N.; Kudin, K. N.; Staroverov, V. N.; Kobayashi, R.; Normand, J.; Raghavachari, K.; Rendell, A. P.; Burant, J. C.; Iyengar, S. S.; Tomasi, J.; Cossi, M.; Rega, N.; Millam, N. J.; Klene, M.; Knox, J. E.; Cross, J. B.; Bakken, V.; Adamo, C.; Jaramillo, J.; Gomperts, R.; Stratmann, R. E.; Yazyev, O.; Austin, A. J.; Cammi, R.; Pomelli, C.; Ochterski, J. W.; Martin, R. L.; Morokuma, K.; Zakrzewski, V. G.; Voth, G. A.; Salvador, P.; Dannenberg, J. J.; Dapprich, S.; Daniels, A. D.; Farkas, O.; Foresman, J. B.; Ortiz, J. V.; Cioslowski, J.; Fox, D. J. Gaussian 09, revision D. 01. 2009.

(S9) Abraham, M. J.; Murtola, T.; Schulz, R.; Páll, S.; Smith, J. C.; Hess, B.; Lindahl, E. GROMACS: High performance molecular simulations through multi-level parallelism from laptops to supercomputers. *SoftwareX* **2015**, *1*, 19–25.

(S10) Kirschner, K. N.; Yongye, A. B.; Tschampel, S. M.; González-Outeiriño, J.; Daniels, C. R.; Foley, B. L.; Woods, R. J. GLYCAM06: a generalizable biomolecular force field. Carbohydrates. *J. Comput. Chem.* **2008**, *29*, 622–655.

(S11) Tribello, G. A.; Bonomi, M.; Branduardi, D.; Camilloni, C.; Bussi, G. PLUMED 2: New feathers for an old bird. *Comput. Phys. Comm.* **2014**, *185*, 604–613.

(S12) Wassenaar, T. A.; Ingólfsson, H. I.; Bo ckmann, R. A.; Tieleman, D. P.; Marrink, S. J. Computational lipidomics with insane: a versatile tool for generating custom membranes for molecular simulations. *J. Chem. Theory Comput.* **2015**, *11*, 2144–2155.

(S13) Wassenaar, T. A.; Pluhackova, K.; Böckmann, R. A.; Marrink, S. J.; Tieleman, D. P.

Going Backward: A Flexible Geometric Approach to Reverse Transformation from Coarse Grained to Atomistic Models. *J. Chem. Theory Comput.* **2014**, *10*, 676–690.

(S14) Van Der Walt, S.; Colbert, S. C.; Varoquaux, G. The NumPy array: a structure for efficient numerical computation. *Comput. Sci. Eng.* **2011**, *13*, 22–30.

(S15) Humphrey, W.; Dalke, A.; Schulten, K. VMD: visual molecular dynamics. *J. Mol. Graphics Modell.* **1996**, *14*, 33–38.

(S16) Schrödinger, L. The PyMOL Molecular Graphics System, Version 1.8. 2015.

(S17) Hunter, J. D. Matplotlib: a 2D graphics environment. *Comp. Sci. Eng.* **2007**, *9*, 90–95.

Figure S1: Definition of the octant sign method. The three chelating rings are represented as thick lines. The signs of each coordinate x, y and z is represented for each octant; the sign of the octant is the product of these signs.

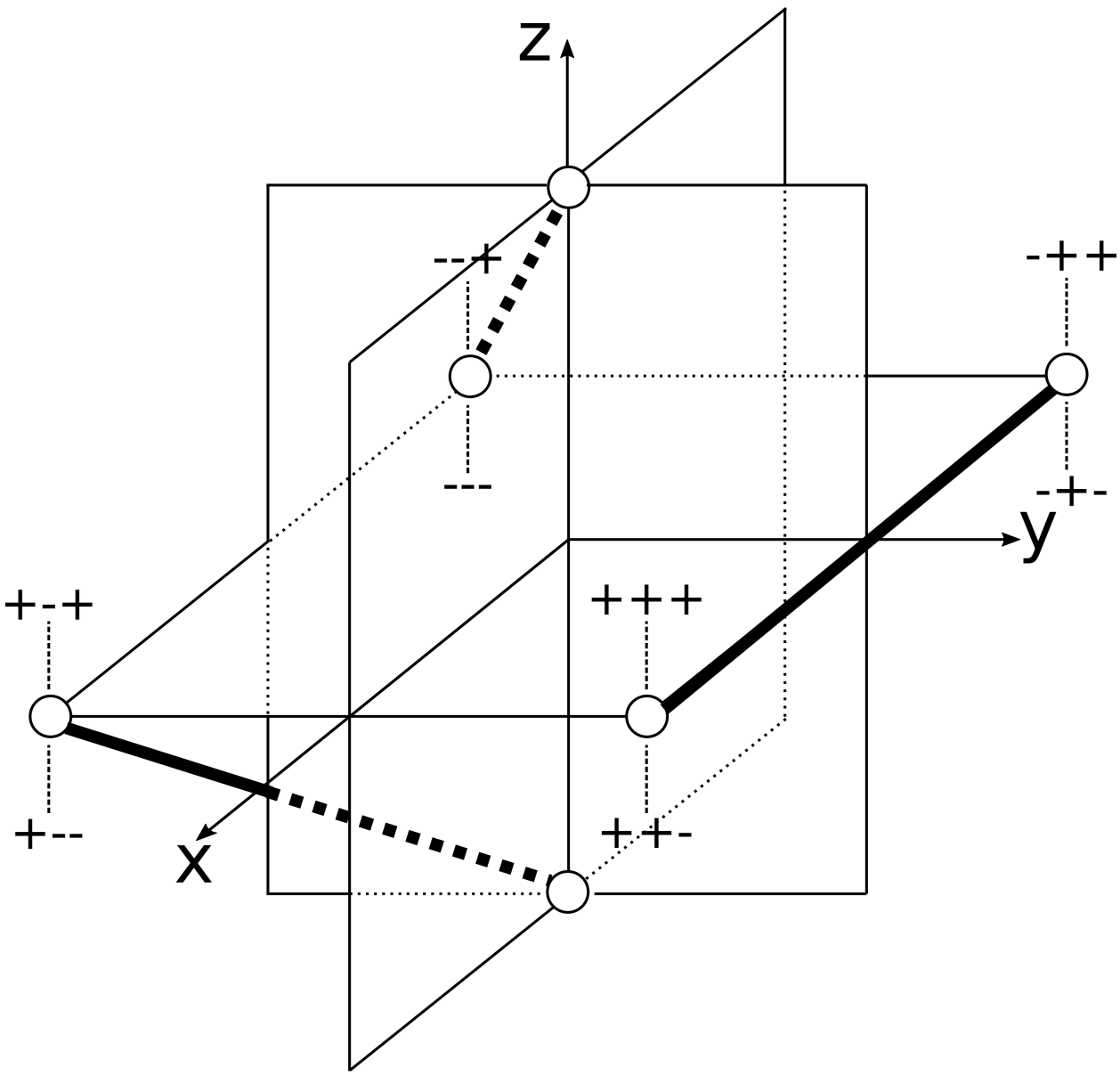

Figure S2: Comparison of the octant and plane methods of determining the chirality of pyoverdine/Fe^{3+} complexes to the dihedral angle Φ used in this study. As can be seen, enantiomers identified as Λ (resp. Δ) by the angle Φ exclusively have their second and third donor rings in positive (resp. negative) octants, and feature coplanar atoms aABc, abBc and AbcC (planes p1, p2, p3) (resp. aBCc, AaCb, ABbc – planes p4, p5, p6). Values of Φ around 0 correspond to confomations which deviate from hexacoordinated geometries for which the octant and plane methods were designed; nevertheless, both these two methods as well as the angle Φ behave graciously for such conformations, faithfully reporting conformations as neither Λ nor Δ.

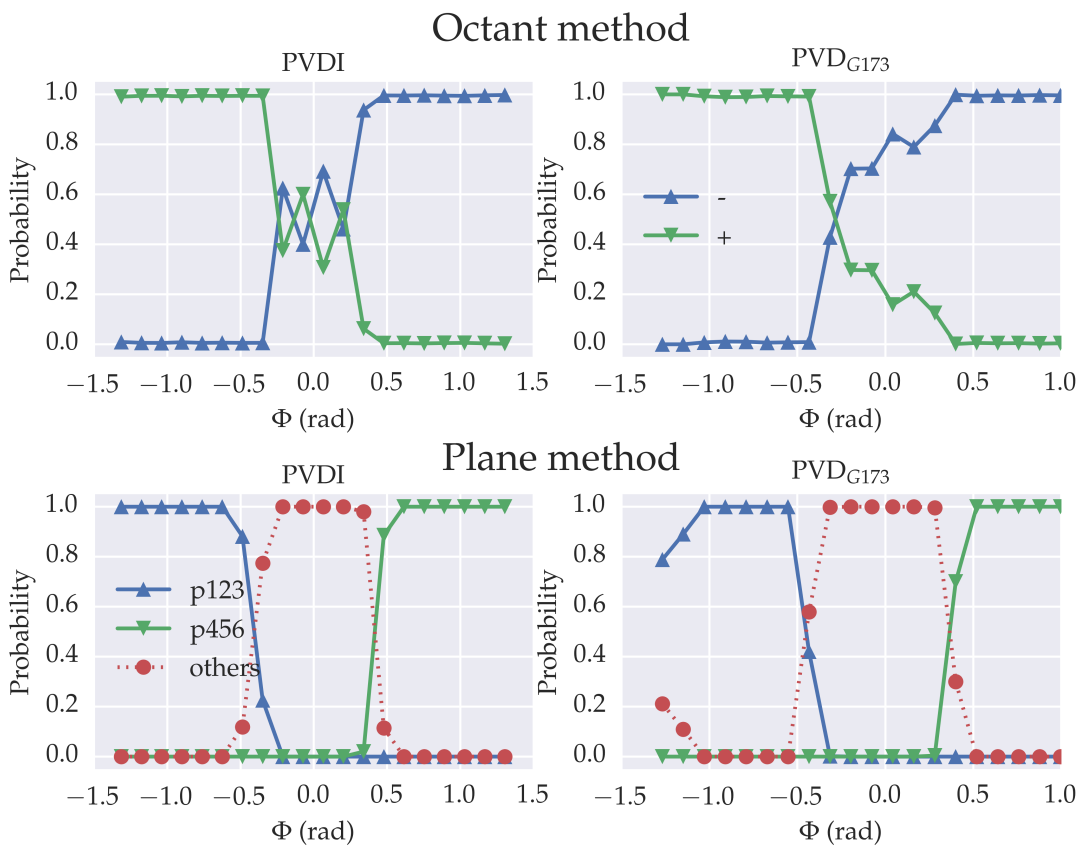

Figure S3: Statistics of Φ during standard (non-biased) molecular dynamics simulations of (from top to bottom) Λ PVDI, Δ PVDI, Λ PVD_{G173} and Δ PVD_{G173}, free or bound to FpvA. Left panels: histograms of angles (ACca), (CBbc) and (BAab); right panels: histograms of absolute values of all possible differences between angles (ACca), (CBbc) and (BAab).

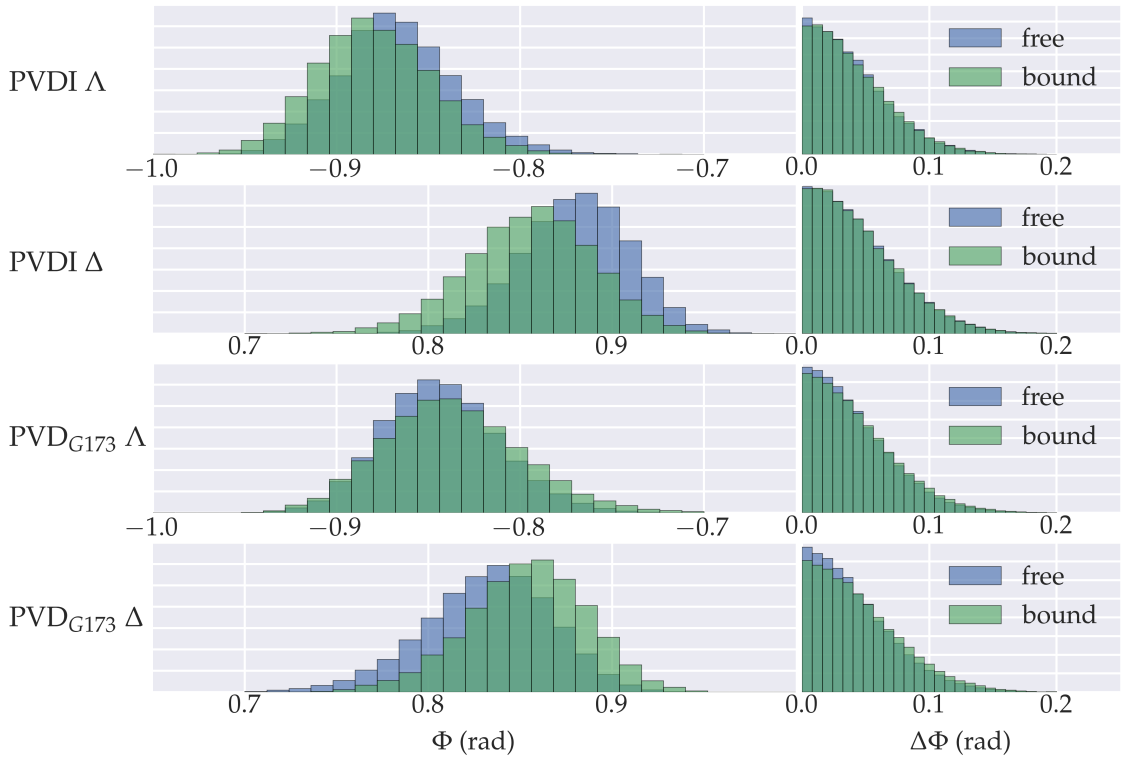

Figure S4: Convergence of well-tempered metadynamics simulations. For each siderophore under study, whether free or bound to FpvA, the absolute value of the difference in free energy of the Δ and intermediate conformers with respect to the Λ conformer is plotted as a function of simulation length.

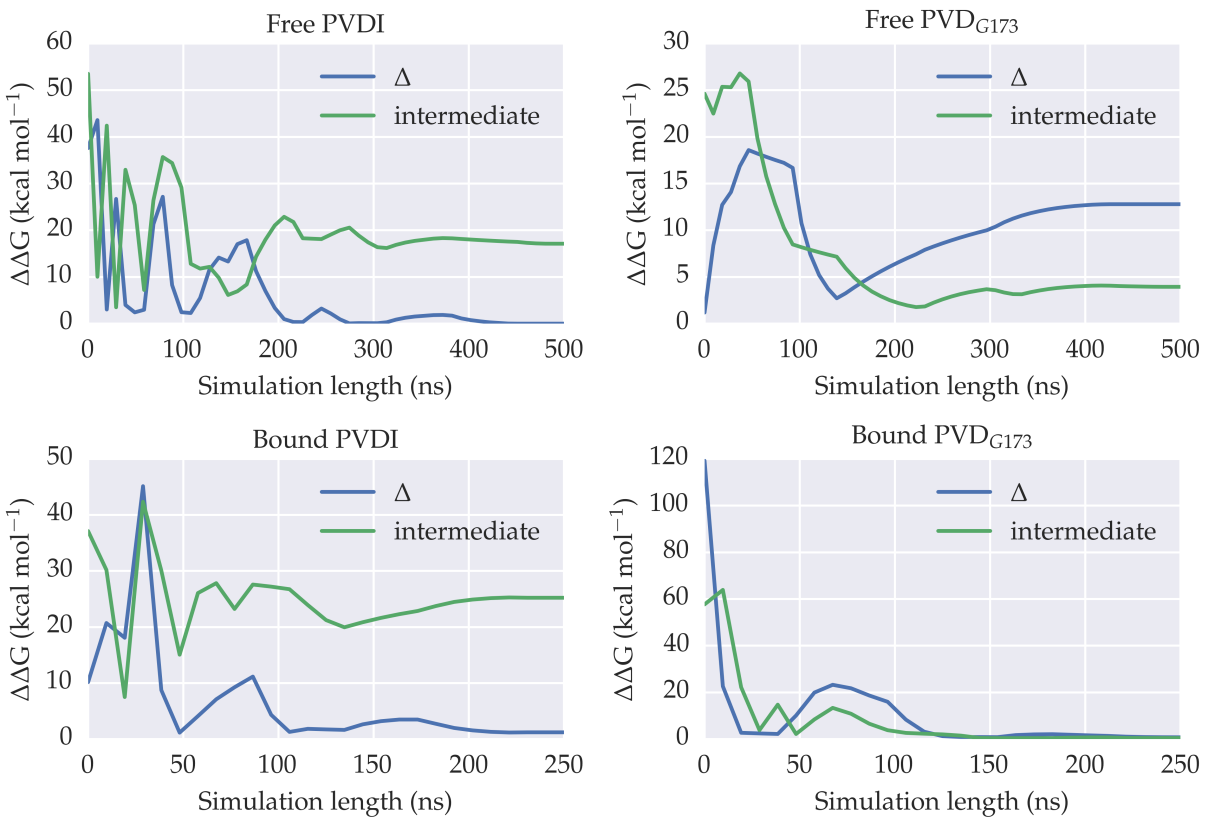

Figure S5: Superposition of representative free (green) and FpvA-bound (cyan) structures of the Λ, intermediate and Δ conformers of PVDI, seen from two different viewpoints (left and right panels).

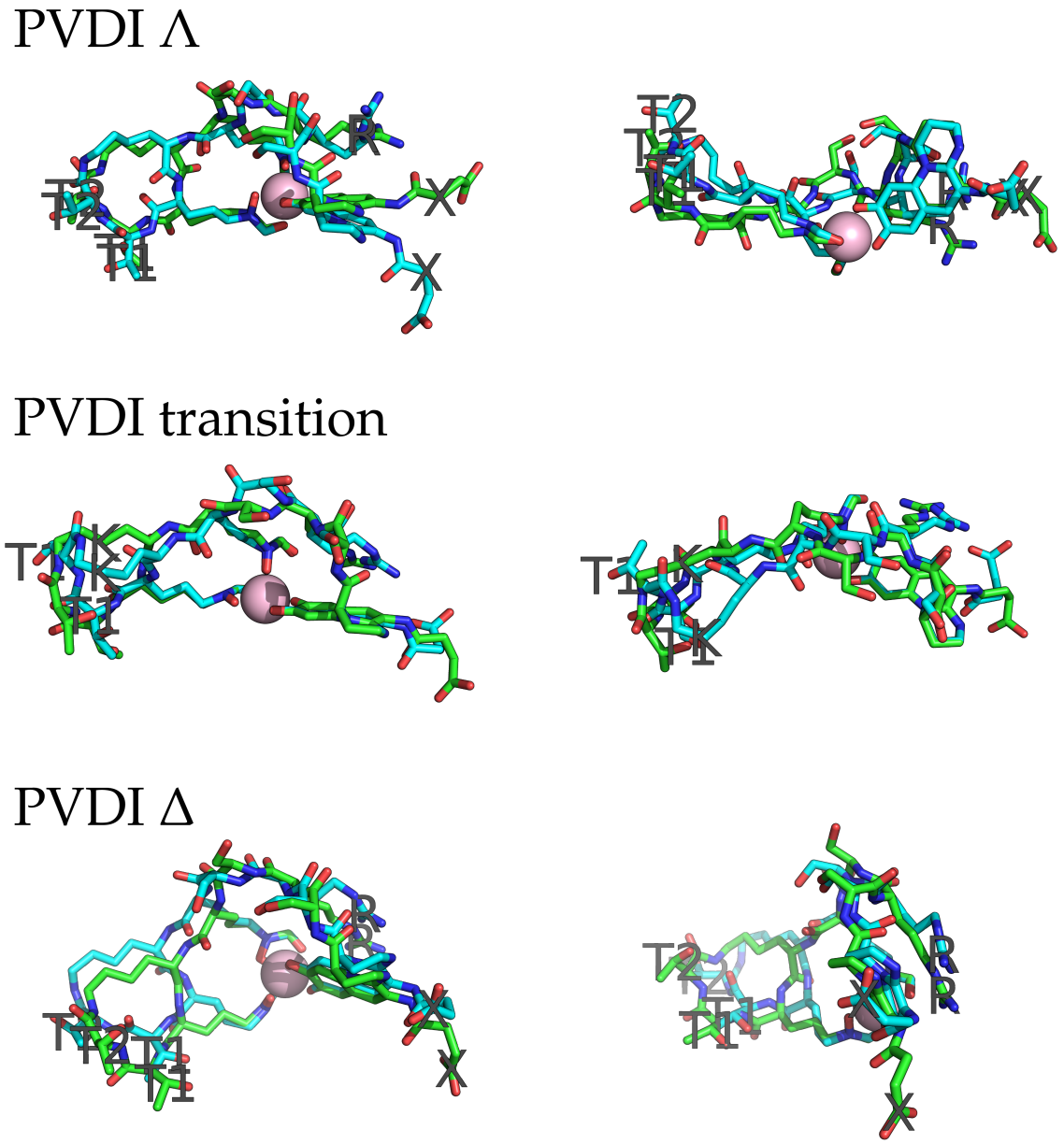

Figure S6: Superposition of representative free (green) and FpvA-bound (cyan) structures of the Λ, intermediate and Δ conformers of PVD_{G173}, seen from two different viewpoints (left and right panels).

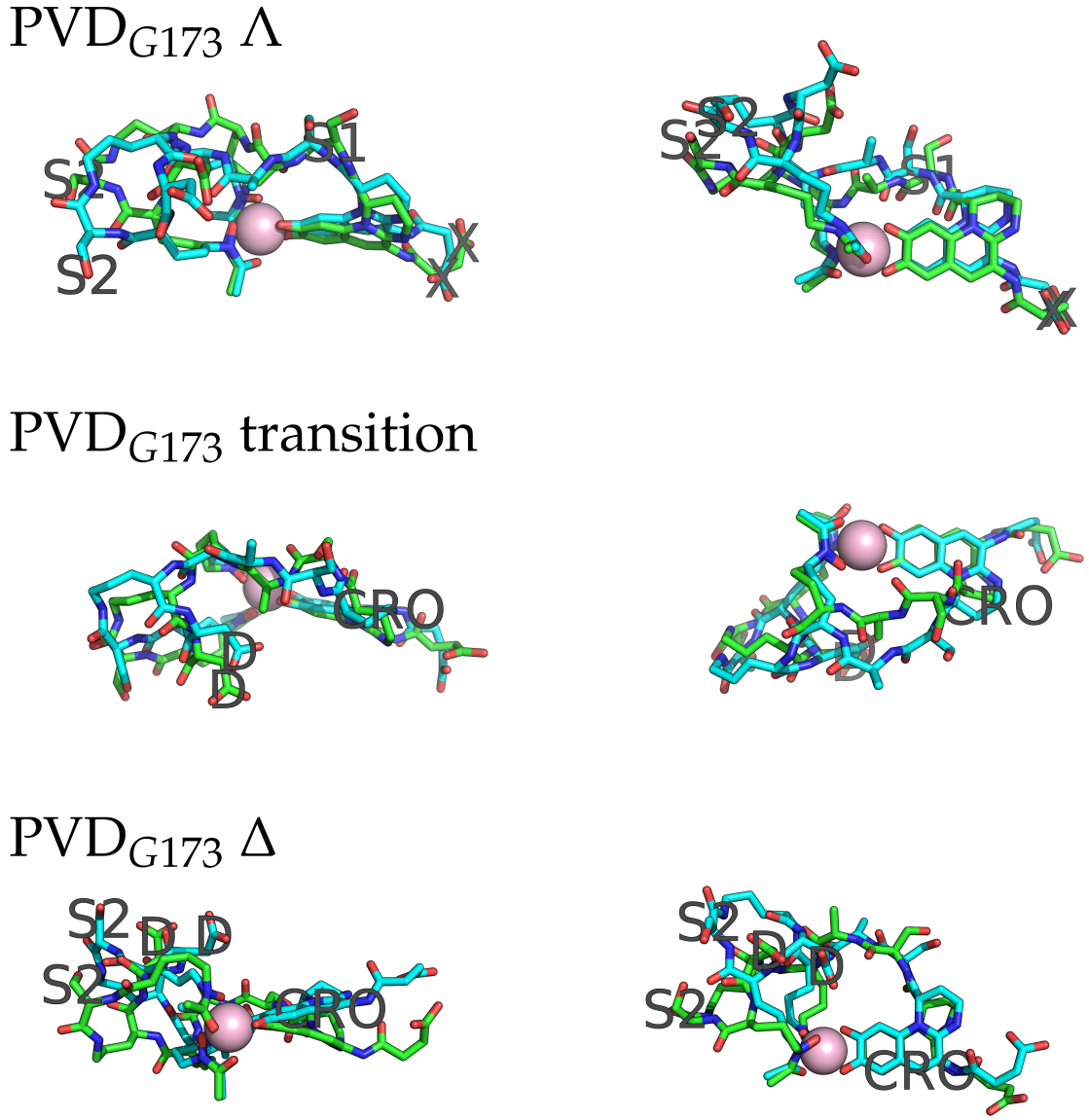

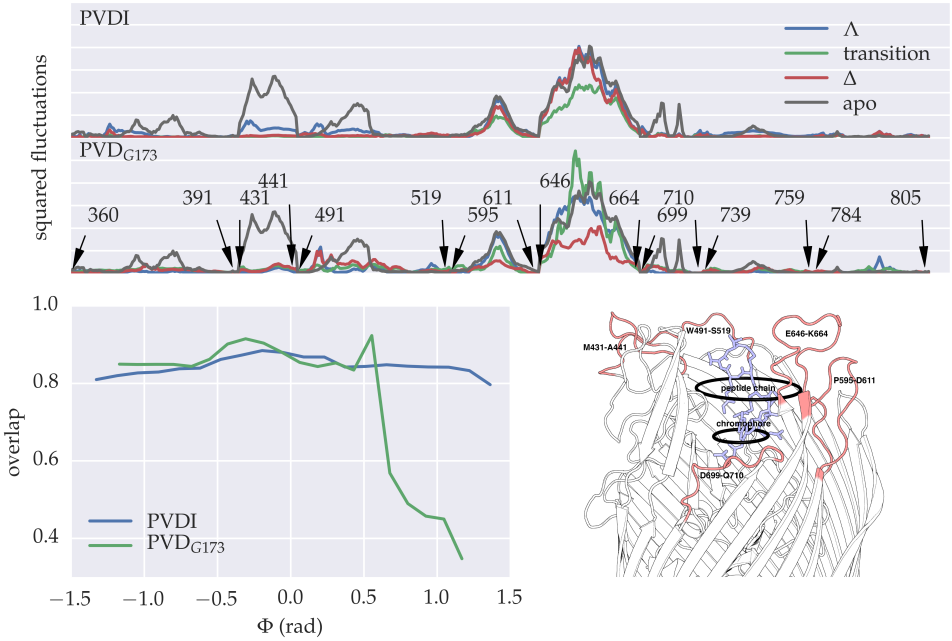

Figure S7: Top: squared fluctuations of the FpvA lid backbone atoms (x axis, identified using residue numbers) along the combined first two PCA eigenmodes for FpvA bound to PVDI and PVD$_{G173}$ (Λ, transition and Δ states) and *apo*-FpvA. Bottom left: overlap between the first PCA eigenmode of the lid of FpvA bound to PVDI and PVD$_{G173}$, and the first five eigenmodes of the lid of *apo*-FpvA, as a function of Φ; this shows that the nature of the correlated motion of the loop atoms is very different in Δ PVD$_{G173}$ compared to other chiralities and siderophores. Bottom right: cartoon representation of FpvA; red: lid loops exhibiting varying flexibilities, with corresponding residue spans; blue: bound pyoverdine, with chromophore and peptide chain regions identified.